ORIGINAL RESEARCH

Pathological Remodeling of Mitral Valve Leaflets from Unphysiologic Leaflet Mechanics after Undersized Mitral Annuloplasty to Repair Ischemic Mitral Regurgitation

Alicja Sielicka, PhD; Eric L. Sarin, MD; Weiwei Shi, MD, PhD; Fatiesa Sulejmani, MS; Daniella Corporan, BS; Kanika Kalra, MD; Vinod H. Thourani, MD; Wei Sun, PhD; Robert A. Guyton, MD; Muralidhar Padala, PhD

***Background*—**Undersized ring annuloplasty is a commonly used surgical repair for ischemic mitral regurgitation, in which annular downsizing corrects regurgitation, but alters valve geometry and elevates tissue stresses. In this study, we investigated if unphysiological leaflet kinematics after annuloplasty might cause pathogenic biological remodeling of the mitral valve leaflets, and if preserving physiologic leaflet kinematics with a better technique can moderate such adverse remodeling.

***Methods and Results*—**Twenty-nine swine were induced with ischemic mitral regurgitation, and survivors were assigned to groups: 7 underwent annuloplasty, 12 underwent annuloplasty with papillary-muscle approximation, 6 underwent papillary-muscle approximation, and 3 were sham controls. Pre-and post-surgery leaflet kinematics were measured, and valve tissue was explanted after 3 months to assess biological changes. Anterior leaflet excursion was unchanged across groups, but persistent tethering was observed with annuloplasty. Posterior leaflet was vertically immobile after annuloplasty, better mobile with the combined approach, and substantially (P=0.0028) mobile after papillary-muscle approximation. Procollagen-1 was higher in leaflets from annuloplasty compared with the other groups. Heat shock protein-47 and lysyl oxidase were higher in groups receiving annuloplasty compared with sham. α-SMA was elevated in leaflets from animals receiving an annuloplasty, indicating activation of quiescent valve interstitial cells, paralleled by elevated transforming growth factor-β expression.

***Conclusions*—**This is the first study to demonstrate that surgical valve repairs that impose unphysiological leaflet mechanics have a deleterious, pathological impact on valve biology. Surgeons may need to consider restoring physiologic leaflet stresses as well as valve competence, while also exploring pharmacological methods to inhibit the abnormal signaling cascades. **(*J Am Heart Assoc*. 2018;7:e009777. DOI: 10.1161/JAHA.118.009777)**

Key Words: animal model surgery • mitral valve regurgitation • mitral valve repair, mitral annuloplasty, subannular repair, mitral valve fibrosis, heart valve repair durability, mitral valve

Undersized ring annuloplasty (URA) is a frequently used surgical technique to repair ischemic mitral regurgitation (IMR), in which a malleable annuloplasty ring is implanted onto the mitral valve (MV) to downsize the dilated mitral annulus and restore leaflet coaptation[1] (Figure 1A). Despite achieving valve competence and an acutely satisfactory hemodynamic outcome, this approach results in an unphysiological MV configuration, with a hyperextended anterior leaflet (AL) and a vertically immobilized posterior leaflet (PL) after the repair[2–4] (Figure 1B). Both AL and PL are tethered in diastole and systole and are under chronic tethering. This unphysiological leaflet configuration induces pathological stresses on the MV leaflets and redistribution of chordal forces, which may incite pathological remodeling such as thickening, fibrosis, and calcification (Figure 1C). Though supportive pathological studies are lacking on this topic prior

From the Structural Heart Research & Innovation Laboratory, Carlyle Fraser Heart Center, Emory University Hospital Midtown, Atlanta, GA (A.S., E.L.S., W.W.S., D.C., K.K., V.H.T., R.A.G., M.P.); Department of Cardiothoracic Surgery, Inova Heart and Vascular Institute, Fairfax, VA (E.L.S.); Wallace H. Coulter Department of Biomedical Engineering, Georgia Institute of Technology, Atlanta, GA (F.S., W.S.); Department of Cardiac Surgery, MedStar Heart and Vascular Institute and Georgetown University, Washington, DC (V.H.T.); Division of Cardiothoracic Surgery, Joseph P. Whitehead Department of Surgery, Emory University School of Medicine, Atlanta, GA (R.A.G., M.P.).

Correspondence to: Muralidhar Padala, PhD, Structural Heart Research and Innovation Laboratory in the Cardiothoracic Research Laboratories, Carlyle Fraser Heart Center, Division of Cardiothoracic Surgery, Emory University School of Medicine, 380B Northyards Blvd, Atlanta, GA 30313. E-mail: spadala@emory.edu

Received July 31, 2018; accepted October 3, 2018.

Clinical Perspective

What Is New?

- In this study, we demonstrate that undersized ring annuloplasty, a standard foundational component of mitral valve repair, that restores acute valve competence but at the expense of valve tethering and abnormal valve mechanics, induces fibrotic remodeling and stiffening in the mitral valve leaflets.
- To our knowledge, this report for the first time demonstrates that unphysiological valve mechanics imposed by surgical repairs can induce pathological valve remodeling, which may contribute to poor durability of the mitral repair.
- The pathogenic mechanisms identified can be targeted with drugs, opening a potential avenue to modulate post-repair valve tissue properties and improve durability.

What Are the Clinical Implications?

- In current practice, there are scant data of changes in the valve leaflet structure and biology resulting from surgical repairs that impose abnormal valve mechanics.
- The results from this study may spark interest in the deleterious effect that valve surgery may have on valve biology and encourage surgeons to consider repairing valves to preserve native valve mechanics, in addition to restoring valve competence.
- These results may provide an explanation for poor durability of current surgical repairs, and spark interest in further studies to use drugs alongside surgery to inhibit postsurgical valve remodeling.

to this study, such leaflet changes have been reported in patients at the time of reoperation for failure of a previous URA repair.[5] Suh et al, performed serial cardiac computed tomography 1 to 5 years postoperatively to assess the MV in 45 patients and demonstrated that leaflet thickening occured in 69% of patients.[6] Those patients with thicker leaflets also presented with elevated transmitral pressure gradients, indicating progressive valve stenosis.

The link between elevated mechanical strain and fibroblasts was explored earlier in valvulogenesis, heart failure, and benchtop models of valve disease. Quick and Kunzelman reported that MV leaflets with abundant fibroblast-like valve interstitial cells have altered collagen concentration when subjected to mechanical strain.[7,8] Grande-Allen et al found that in heart failure patients with chronic MV tethering and systemic inflammation, the leaflets are significantly thicker and stiffer.[9,10] In a more recent series of investigations, Dal-Bianco et al demonstrated that tethering and inflammation have a dual mode effect on activating MV interstitial cells.[11] Their work demonstrated that not only are interstitial fibroblasts activated in the presence of stretch, but endothelial cells trans-differentiate into interstitial like cells that can synthesize collagen and transforming growth factor-β (TGFβ) in their microenvironments.[12] Shapero et al in a cell culture model demonstrated that activation of the endothelial and interstitial cells occurs in a reciprocal manner,[13] and Bartko et al demonstrated the potential to modulate the profibrotic changes in the mitral valve with Losartan.[14]

This increasing evidence on the mechano-sensitivity of valves led us to hypothesize that surgical repairs that do not restore physiological leaflet configuration and demonstrate elevated mechanical strains, could induce pathogenic biological changes in valve leaflets. In a previous report, we demonstrated that MV mechanics and geometry after repair with URA are highly unphysiological, with AL hyperextension and posterior leaflet immobility in a bench model.[15] In this study, we used a clinically relevant swine model of chronic moderate IMR[16] to investigate if URA-imposed abnormal valve kinematics can induce biological changes to the leaflets. To determine if valve kinematics are the primary drivers of such leaflet remodeling, we compared valves after URA with valves from animals that underwent sub-leaflet papillary muscle approximation (PMA) as well. We[17,18] and others[19,20] have recently demonstrated that PMA is a simple technique that partially restores physiological leaflet kinematics when performed with URA, but fully restores native valve-like function when performed in isolation. By comparing leaflet biological changes with URA, URA+PMA, PMA and an unrepaired sham, we sought to delineate the potential pathogenic drivers of this novel phenomenon that has not been previously explored.

Methods

The methods, and materials will be provided to other researchers for purposes of replicating the results upon request.

Experimental Design

A chronic swine model of IMR that was previously described and in which moderate IMR was confirmed with multiple modalities was used[16] (Figure 2). Yorkshire farm swine (n=29, male, 38±5.1 kg) were induced with a myocardial infarction and allowed to develop IMR over 2 months. Moderate IMR was confirmed and the 28 surviving animals were randomly assigned to 4 groups: (group 1, n=3) Control (no mitral repair); (group 2, n=7) URA only; (group 3, n=12) URA with sub-annular PMA; and (group 4, n=6) PMA only. Of the 12 pigs in the URA+ sub-annular PMA group, 7 survived the entire chronic follow-up and were used in this study. None of the surviving pigs were omitted from the study, as all of them developed moderate MR in this model as described and validated previously.[16] Techniques used to perform these repairs are identical to those in humans and were reported

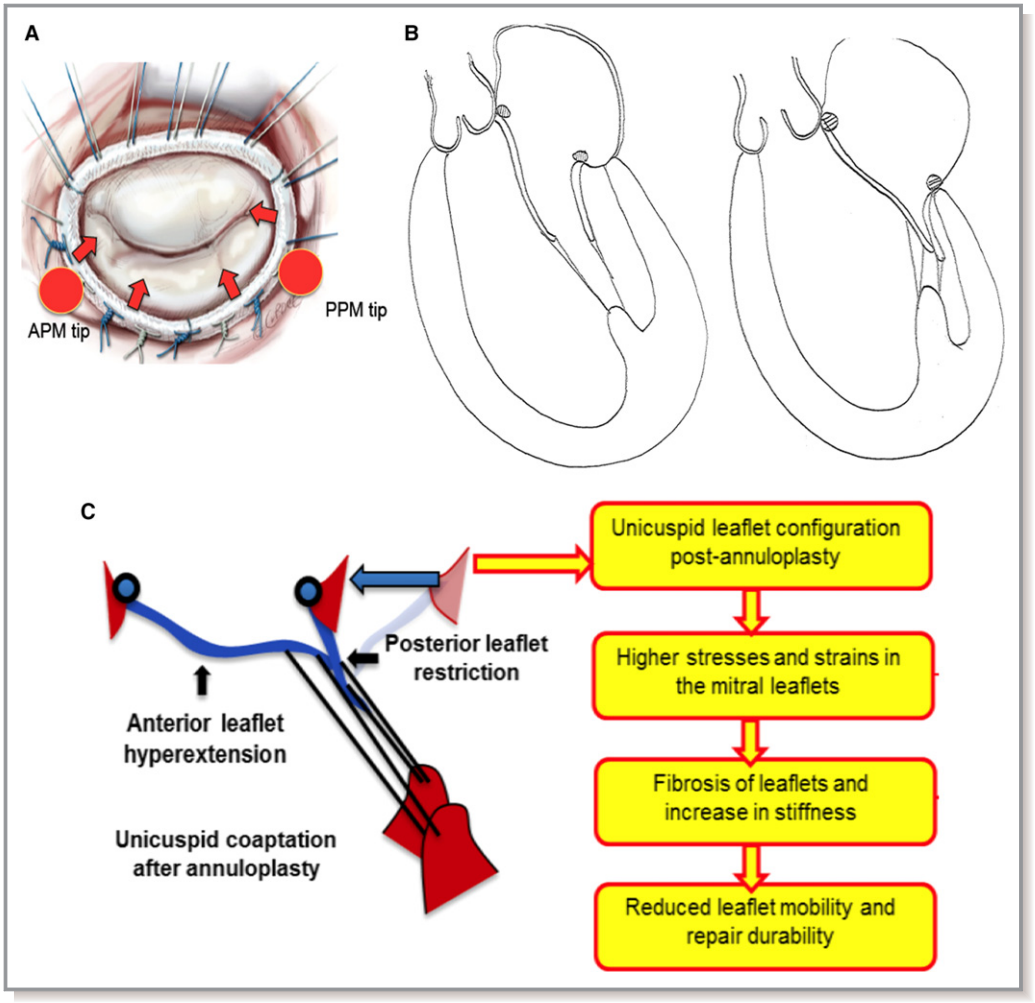

Figure 1. **A**, Schematic depicting undersizing mitral annuloplasty on a mitral valve, in which the ring draws the leaflets inwards into the mitral orifice because of its smaller size, but away from both the papillary muscle tips, resulting in tethering of both the leaflets. **B**, Drawings depicting the typical diastolic and systolic leaflet configuration evident after undersizing mitral annuloplasty. **C**, Schematic depicting the pathological leaflet remodeling hypothesis from the unphysiological force distribution on the mitral valve leaflets after repair with undersizing annuloplasty. APM indicates anterior papillary muscle; PPM, posterior papillary muscle.

earlier.[21] The pigs were survived for an additional 3 months after the surgery, and MV tissue was harvested at termination and assigned to different assays that were used to quantify leaflet matrix remodeling and fibrosis.

Animal Procedures

Procedures were approved by the institutional animal care and use committee (IACUC) and performed at an Association for Assessment and Accreditation of Laboratory Animal Care (AALAC) accredited facility. Pigs were purchased from Valley Brook Farms, GA or Palmetto Farms, SC, vaccinated, and acclimated to our facility. The animals were pair housed until surgery, with continuous access to drinking water and fed a standard chow (14% crude protein, 3% crude fat, 0.6% calcium, 0.65% phosphorus, 0.3% salt, and 166 ppm zinc mixed in 14% hog finisher from Tucker Milling, Guntersville, AL).

IMR Model

Techniques to induce IMR were described in a previous publication,[16] and its severity was validated with different techniques. A large postero-lateral myocardial infarction was induced by percutaneous intracoronary thrombosis of the obtuse marginal branches of the left circumflex artery. The drugs used for the myocardial infarction procedure are listed in Table. The pigs were intubated and mechanically ventilated. The groin and neck areas were shaved, cleaned, and sterile draping was performed. Right femoral and carotid arterial cut downs were performed to insert two 8Fr vascular sheaths (Super Sheath, Boston Scientific). A 6Fr pigtail catheter (SiteSeer, Medtronic) was inserted into the left ventricle via the carotid sheath, and a 7Fr hockey stick catheter (VistaBrite, Cordis) was inserted retrograde into the coronary ostia. The posteromedial papillary muscle was identified on the left ventriculogram and

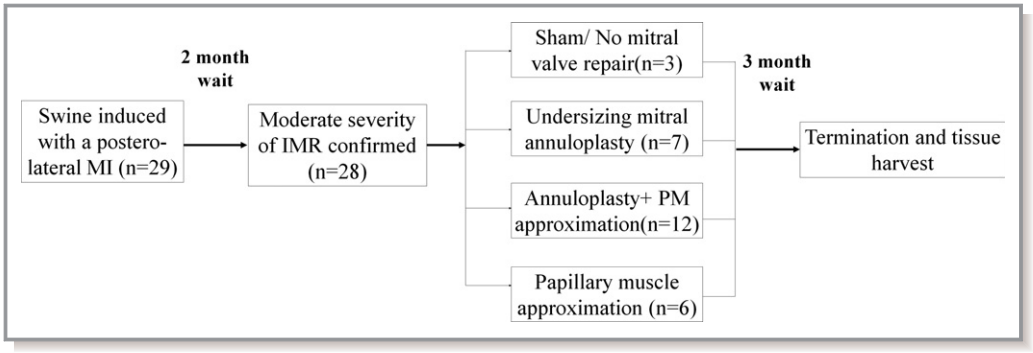

Figure 2. Experimental design of the study, depicting assignment of pigs to different experimental groups and the wait time between each step. IMR indicates ischemic mitral regurgitation; MI, myocardial infarction.

the left circumflex arterial branches perfusing it and the entire postero-lateral myocardium were marked. A coronary artery dilation balloon (Mini Trek Coronary Dilatation Balloon, Abbott Vascular) was advanced over a 0.014″ guidewire into the target vessels and inflated to isolate the vasculature and 100% (200 proof) ethanol was injected into these arteries. The balloon was left inflated for 20 minutes, for complete thrombosis, and was confirmed with a repeat angiogram. S-T elevation was confirmed, the incisions were closed, and the animal was recovered from anesthesia. Each pig was individually housed, and echocardiography was performed to confirm moderate IMR at 2 months postprocedure.

Mitral Valve Repair

Cardiopulmonary bypass techniques for MV repair were described in an earlier publication.[21] A left thoracotomy was performed between the fourth and fifth intercostal space, a pericardial cradle was made and the heart was exposed. Baseline echocardiography was performed to confirm IMR. Arterial cannulation in the mid-ascending aortic arch was performed with a 21Fr EZ glide right-angled cannula and venous cannulation was performed in the right atrial appendage with a dual stage 29/37Fr cannula. A cardioplegia catheter was inserted into the aortic root and adenocaine was infused for cardiac arrest. Upon clamping the aorta, a left atriotomy was performed, blood was suctioned with a sucker left in the pulmonary vein and the MV was exposed. In group 2, a URA ring (24 mm Edwards Physio II annuloplasty ring) was implanted with ten 2-0 Ethibond annular sutures; in group 3, in addition to URA, PMA was performed with a pledgeted 3-0 prolene, and the papillary muscle heads and 1 cm of their body were approximated; and in group 4, only PMA was performed. Group 1 animals were used as sham controls that did not undergo any surgery. After the mitral procedure, the left atriotomy was closed, and the animal was gradually

Table. Medications Used in Swine for the Duration of the Study, Segregated into Those Relevant to the Ischemic Mitral Regurgitation Induction Procedure and Those Relevant to the Mitral Valve Repair Procedure

Ischemic Mitral Regurgitation Procedure				Mitral Valve Repair Procedure			
Drug	Dosage/Frequency	Route	Purpose	Drug	Dosage/Frequency	Route	Purpose
Amiodarone	600 mg SID, 3 d prior	PO	Anti-arrhythmic	Aspirin	81 mg SID, 3 d prior	PO	Anti-platelet
Aspirin	81 mg SID, 3 d prior	PO	Anti-platelet	Plavix	75 mg SID, 3 d prior	PO	
Plavix	75 mg SID, 3 d prior	PO		Solumedrol	200 to 500 mg, once	IV	Anti-inflammatory
Ketamine	22 mg/kg, once	IM	Sedative cocktail	Cefazolin	22 to 25 mg/kg, once before surgery and then PRN	IV	Antibiotic
Acepromazine	1.1 mg/kg, once	IM		Carprofen	3 mg/kg, once before surgery and then PRN	IV	NSAID
Atropine	0.05 mg/kg, once	IM		Ketamine	22 mg/kg, once	IM	Sedative cocktail
Isoflurane	1% to 2% in 100% oxygen	Inhalant	Anesthetic	Acepromazine	1.1 mg/kg, once	IM	
Amiodarone	8 mg/kg	IV	Anti-arrhythmic	Atropine	0.05 mg/kg, once	IM	
Cefazolin	22 to 25 mg/kg	IV	Antibiotic	Isoflurane	1% to 2% in 100% oxygen	Inhalant	Anesthetic
Carprofen	3 mg/kg	IV	NSAID	Euthasol	80 mEq	IV	Termination

IV indicates intra venous; IM, intra muscular; PO, per os (i.e. drug given orally); PRN, pro re nata (as needed); SID, Semel in Die (once a day).

weaned from bypass and decannulated. The thoracotomy was closed, a temporary chest tube was placed, and the animal was fully recovered with supplemental oxygen, inotropes as needed, and with adequate analgesics.

Cardiac Imaging

Echocardiography was performed before and after surgery. Individual leaflet tethering areas and excursion angles were measured from the echocardiography images by a blinded echocardiographer using a GE Vivid I system. Cardiac magnetic resonance imaging was performed in 1 swine in each group, to confirm the differences in the leaflet configuration between the groups (Figure 3A). The parameters measured before and after surgery using cardiac echocardiography are depicted in Figure 3B.

Necropsy and Tissue Collection

Swine were terminated under anesthesia with 80 mEq of euthasol (pentobarbital sodium and phenytoin sodium) after heparinization. The heart was harvested, and the AL and PL were explanted without the chordae tendineae, and sections were cut to a predetermined length. Some tissue from each leaflet was preserved in cold saline for biaxial mechanical testing, some was snap frozen in liquid nitrogen at −80°C, and some stored in 10% formaldehyde.

Biological Assays

Gene expression PCR arrays

AL and PL from 3 individual pigs in each group were used to perform polymerase chain reaction (PCR) arrays to probe for 84 extracellular and adhesion molecule genes (PASS-130Z, Qiagen). Three arrays for the AL and three for the PL in each group were used, resulting in a total of 24 arrays for the study. Thirty milligrams of leaflet tissue from each pig was homogenized, and total RNA was extracted with RiboPure RNA Purification Kit (AM1924, Thermo Fisher), with the concentration and purity determined with a spectrophotometer (Synergy HT, BioTek). For each sample 0.5 μg of total RNA was reverse transcribed with a reverse transcription mix (330401, Qiagen). The reaction was performed at 42°C for 15 minutes, and at 95°C for 5 minutes (MJMini, BioRad). PCR components were mixed for each 96-well plate: 1350 μL 2xRT^2 SYBR Green Mastermix, 102 μL cDNA synthesis reaction and 1248 μL RNase-free water (330523, Qiagen). Twenty-five microliters of PCR components were added to each well, and the plates were centrifuged for 1 minute at 1000 g at room temperature. PCR reaction was performed at 95°C for 10 minutes; 95°C for 15 seconds, and 60°C for 1 minute, for 40 cycles each (StepOnePlus, Applied Biosystems). Real-time quantitative PCR reaction was performed in a 96-well plate array consisting of pig extracellular matrix (ECM) genes, adhesion genes and fibrosis pathway genes. Fold-change calculations were performed from the threshold cycle data, using a web-based software, and validated using 5 housekeeping genes (actin gamma 1 (ACTG1), beta 2 microglobulin (B2M), glyceraldehyde 3-phosphate dehydrogenase (GAPDH), Hypoxanthine Phosphoribosyltransferase 1 (HPRT1), ribosomal protein L13A (RPL13A)).

Immunoblotting

Four to 6 individual samples were used per group for immunoblotting of each protein involved in collagen synthesis, while 3 to 4 individual samples were used per group for active and total TGFβ immunoblotting. Frozen tissue was thawed, weighed and equal parts homogenized in tissue extraction reagent 1 (50 mmol/L Tris [hydroxymethyl]aminomethane, pH 7.4, 250 mmol/L sodium chloride [NaCl], 5 mmol/L ethylenediaminetetraacetic acid [EDTA], 2 mmol/L sodium orthovanadate [Na_3VO_4], 1 mmol/L sodium flouride [NaF], 20 mmol/L sodium pyrophosphate tetrabasic [$Na_4P_2O_7$], 0.02% sodium azide [NaN_3]) with freshly added protease and phosphatase inhibitors in a bead mill. The homogenates were centrifuged at 16200 g at 4°C. Total protein in the lysates were measured with bicinchoninic acid assay (BCA), and equal amount of protein (1 mg/mL) were loaded into each lane of the 12% sodium dodecyl sulfate-polyacrylamide gels, and electrophoresis conducted at 100V (initial current: 15–20 mA; final: 5–10 mA). The proteins were transferred to a polyvinylidene fluoride membrane, blocked with non-fat milk, and incubated overnight at 4°C with primary antibody and then with secondary antibody for 1 hour at room temperature (Horseradish peroxidase (HRP)-conjugated anti-mouse or anti-rabbit). Primary antibodies against procollagen 1 C-terminal propeptide (MBS6002643, Mybiosource), procollagen 1 N-terminal propeptide (MBS2004656, Mybiosource), prolyl 4-hydroxylase 1 (MBS128946, Mybiosource), heat shock protein 47 (SC-8352, Santa Cruz Biotechnology), lysyl oxidase (L2623-11, US Biological), and GAPDH (G9295, Sigma-Aldrich) were used. Antigen–antibody complexes were visualized with chemiluminescent substrate and a chemiluminescence-sensitive film. The membrane was stripped and probed with GAPDH antibody to validate equal protein loading. Western blotting for each protein in each sample was performed 4 times, and the data were averaged. Protein levels were determined using densitometry measurements with ImageJ software (National Institutes of Health) and normalized to the level of GAPDH in each sample.

Plasma procollagen

Two milliliters of venous blood was collected into an EDTA tube before surgery and at termination. Plasma was separated by centrifugation for 10 minutes at 1200G at room temperature, and frozen at −80°C. Plasma procollagen-1 terminal N-peptide (PINP) was measured in each sample with an

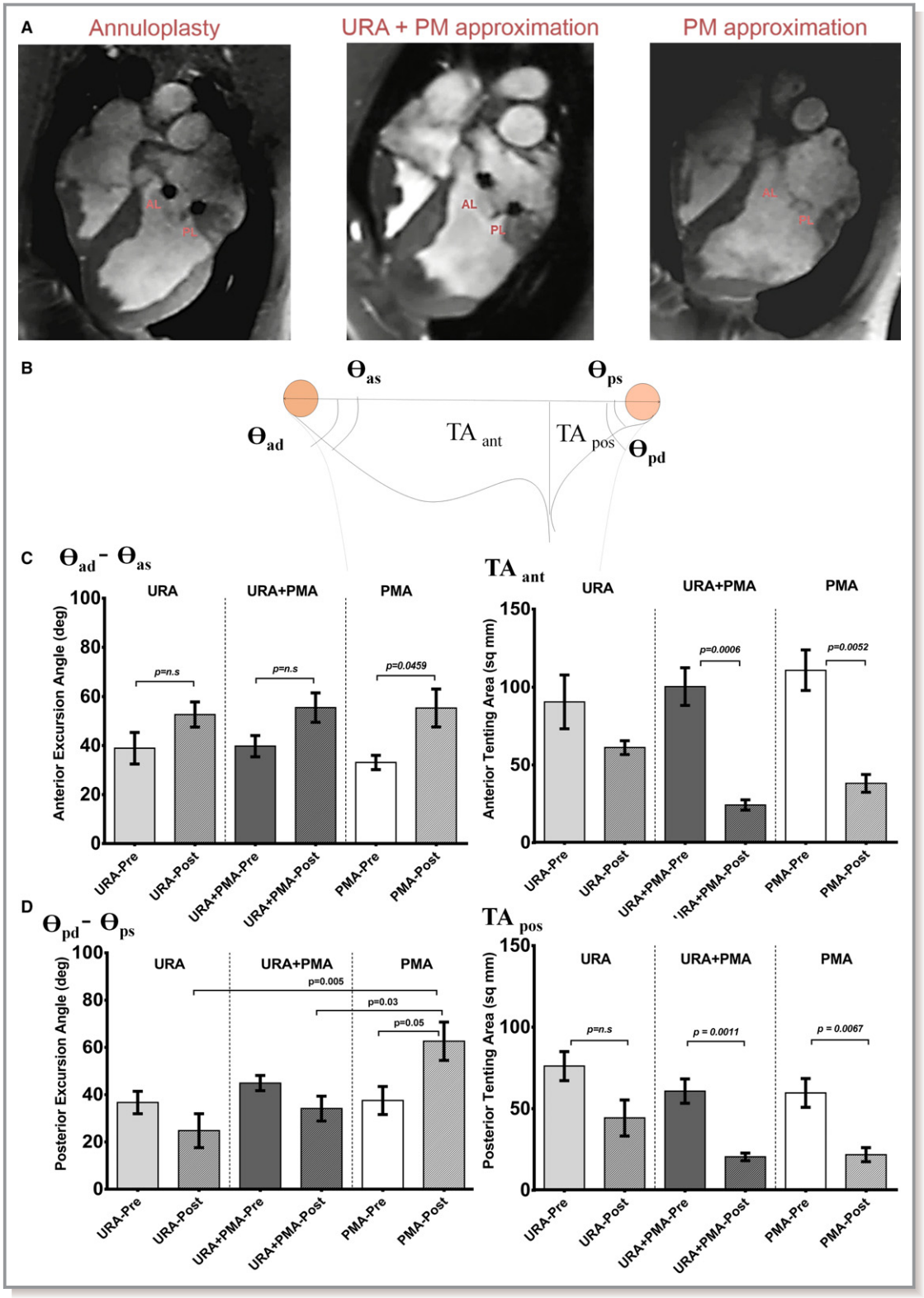

Figure 3. **A**, Differences in systolic and diastolic leaflet configurations between the 3 types of repairs (undersizing ring annuloplasty, undersizing ring annuloplasty+papillary muscle approximation and papillary muscle approximation) as seen on representative magnetic resonance images obtained in a pig in each group. **B**, Parameters measured from the echocardiographic images in each pig before and after surgery. **C**, Differences in the anterior leaflet excursion angle and the anterior tenting area before and after each repair. **D**, Differences in the posterior leaflet excursion angle and the posterior tenting area before and after each repair. AL indicates anterior leaflet; PL, posterior leaflet; PMA, papillary muscle approximation; URA, undersized ring annuloplasty.

enzyme-linked immunosorbent assay (MBS007084, MyBiosource). The detection range of the assay was 6.25 to 200 ng/mL with a sensitivity of 1 ng/mL, and experiments were repeated in triplicate for each sample.

Histopathology

Tissues were fixed in 4% paraformaldehyde, dehydrated through a graded series of ethanol, cleared in xylene, and embedded in paraffin. Cross-sections were cut and stained with hematoxylin and eosin, and Masson's Trichrome stains for histological analysis. Images were captured with Zeiss AxioScope A1 microscope with Zeiss AxioCam MRc digital camera, and image stitching was performed with ZEN 2012 (blue edition, version 1.1.0.0).

Tissue immunohistochemistry

Three to 5 μm sections were cut, mounted onto a coverslip, dried, dehydrated in ethanol, and cleared in xylene. Sections were incubated overnight with anti-TGFβ1 (ab92486, Abcam) primary antibody at 4°C. Sections were washed in Tris-buffered saline (TBS) buffer, incubated with anti-rabbit immunoglobulin G (Biocare Medical, Cat # BRR4009) secondary antibody for 1 hour at room temperature, and washed again with TBS. Slides were visualized with 3,3′-diaminobenzidine tetrahydrochloride (Thermo Fisher Scientific, Cat # 34001). Negative controls were performed without primary antibody incubation. Tissues were analyzed using Zeiss Axio Scope A1 microscope and images were captured with Zeiss AxioCam MRc with ZEN 2012 (blue edition, version 1.1.0.0).

Cellular staining and imaging

Paraffin sections of the posterior and anterior leaflets were deparaffinized with xylene and ethanol. After washing at room temperature for 5 minutes in Tris-buffered saline (TBS), antigens were retrieved by heating the samples to 95°C for 15 minutes in Tris/EDTA buffer (Tris 10 mmol/L, EDTA 1 mmol/L, pH 9.0), in a water bath. After cooling and washing with TBS, the sections were treated with a mixture of 10% bovine serum albumin (Sigma-Aldrich) and 10% goat serum (Invitrogen) diluted in SuperBlock T20 (Thermo Fisher Scientific) at room temperature for 120 minutes to block non-specific protein binding. The treated samples were incubated overnight at 4°C in a dark, humidified chamber with a mixture of 2 primary antibodies diluted with 1% bovine serum albumin : anti-CD90 antibody (R&D Systems; sheep) to phenotype fibroblast cells and anti-α-SMA antibody (Abcam; rabbit) to phenotype myofibroblasts/activated fibroblasts. Sections were then washed with TBS and incubated at room temperature for 60 minutes with a mixture of 2 secondary antibodies: Alexa Fluor488 goat anti-rabbit immunoglobulin G (H+L) conjugate (Abcam) and Northern Lights donkey anti-sheep immunoglobulin G (H+L) conjugate (R&D Systems). Finally, the sections were stained with 4 ,6-diamidino-2-phenylindole (DAPI) (Thermo Fisher Scientific), imaged with an Olympus FV1000 Microscope, and analyzed with Fluoview ver.3.1 Viewer (Olympus).

Biaxial mechanical testing

Homogeneous leaflet samples (10×10 mm^2) were cut from the central A2 and P2 cusps, the chordae tendineae were removed and mounted onto a biaxial testing device for testing using published protocols.[22] The test region was mounted with fish hooks and optical graphite markers were placed in a 2×2 mm^2 region in the center of the sample for tracking strain. With the sample submerged in a 0.9% NaCl/H_2O solution at 37°C, a stress-controlled experimental protocol was used for biaxial testing, controlling the ratio of the Lagrangian stress components T_{11}:T_{22}, with T_{12}=T_{21}=0. Seven testing protocols with stress ratios T_{11}:T_{22}=1:1, 0.75:1, 0.5:1, 0.3:1, 1:0.75, 1:0.5, and 1:0.3 were used after a 30- to 40-cycle preconditioning protocol to reduce the effects of hysteresis. From the biaxial results, the equibiaxial responses from each group were combined and compared for both the anterior and posterior leaflets, respectively. Maximum strain, degree of anisotropy, stiffness, and extensibility were computed. The degree of anisotropy was defined by the ratio of the maximum strain values in the circumferential and longitudinal loading directions; the lower the value, the higher the degree of anisotropy. Stiffness was determined by the tangent modulus, calculated from the slope of the lines fitted to the low and high linear regions of the equibiaxial response curve. Extensibility was defined as the intersection of the line fitted to the high linear region with the strain axis. All results are presented as mean±SE.

Statistical Analysis

To detect a 25% difference in leaflet excursion angle between repair groups with 85% power, a minimum of 5 swine were necessary in each group. To detect similar differences in each repair group when compared with the sham group, 3 swine per group were sufficient. Measurements are presented as mean±SD for all imaging data and mean±SE for immunoblots, after checking normality of the data with D'Agostino-Pearson test. If data were non-normal, data are presented as median with interquartile range. Data were analyzed with GraphPad Prism (GraphPad Software, Inc, version 7.01, US). One-way ANOVA was performed with Tukey's post-hoc test to assess differences between experimental groups. Comparison between pre and post repair timepoints in the same animal were performed with a paired *t*-test. Non-normal data are presented as median with interquartile range, and the Kruskal-Wallis test with Dunn's multiple comparisons test, and Mann-Whitney tests were employed for comparison of groups.

Results

Mitral Repair Outcomes and Leaflet Kinematics

Septal lateral annular dimension (in mm) was measured before and after surgery to quantify the extent of annular reduction in each surgical repair group. In the URA group, presurgical annular dimension was 31.69±4.86 mm, that reduced to 23.92±2.78 mm after surgery (24.5% reduction, P=0.0013); in the URA+PMA group, presurgical annular dimension was 34.01±4.44 mm, that reduced to 22.81±0.89 mm after surgery (32.9% reduction, P=0.006); in the PMA group, pre-surgical annular dimension was 34.35±4.87 mm, and remained at 34.07±2.69 mm after the surgery (0.8% reduction, P=0.999). The average grade of MR across all the groups before surgery was 24.5±0.4%, and was 0% after surgery—indicating that the 3 repairs eliminated mitral regurgitation. At termination recurrent regurgitation was not seen on echocardiogram in any of the repair groups. Representative cardiac magnetic resonance imaging images in Figure 3A depict the differences in the anterior and leaflet configurations between the 3 repair groups, and the echocardiographic measurements are depicted in Figure 3B. Anterior leaflet excursion angle before and after each repair is depicted in Figure 3C, was unchanged in the URA and URA+PMA groups but significantly increased in the PMA group (P=0.045). Anterior leaflet tenting area was significantly reduced after repair with URA+PMA (P=0.0006) and PMA (P=0.0052) (Figure 3C). Posterior leaflet excursion angle was significantly increased from pre-repair to post-repair only in the PMA group (P=0.051), but not in the other repair groups. Post-repair posterior leaflet excursion angle was highest in PMA group and was significantly higher than URA and URA+PMA groups (Figure 3D). Posterior tenting area was also reduced after URA+PMA (P=0.0011) and PMA (P=0.0067), but not in the URA group.

Transcriptional Changes in Extracellular Matrix Encoding Genes

Differential expression of genes in the AL and PL in each repair group, normalized to sham, is shown in Figure 4. In the AL, changes in gene expression were generally higher in the URA and URA+PMA groups as compared with sham (P<0.05) (Figure 4A through 4C). In the URA group, expression of Intercellular adhesion molecule 1 (ICAM1), Integrin subunit alpha M (ITGAM), Integrin subunit beta 3 (ITGB3), matrix metalloproteinase 7, and Tissue inhibitor of matrix metalloproteinase 1 (TIMP1) were significantly elevated. In the URA+PMA group, elevated expression of Hyaluronan synthase 1 (HAS 1), ICAM 1, Integrin subunit alpha 2 (ITGA2), Integrin subunit alpha 8 (ITGA8), ITGAM, Contactin 1 (CNTN1), Selectin P (SELP), Secreted phosphoprotein 1 (SPP1), Thrombospondin 1 (THBS1), and TIMP1 was observed. In the PMA group, HAS1, ITGAM, and Laminin subunit beta 3 (LAMB3) were most elevated. In the PL, changes in gene expression compared with the sham group were minimal in PMA, but significant in URA and URA+PMA (Figure 4D through 4F). In these 2 later repair groups, genes encoding different collagens, non-collagen extracellular matrix markers, thrombospondins, and inflammatory proteins were elevated.

Collagen Proteins and Their Chaperones

In general, protein levels of collagen and the chaperones that are involved in collagen synthesis were elevated in all the repair groups compared with the sham group. To highlight differences between the repair groups, the data were normalized to the sham group and the 3 repair groups were compared. Procollagen-1 terminal C-peptide (PICP) and procollagen-1 terminal N-peptide (PINP) are 2 ends of the same immature procollagen protein synthesized by the cells and released into the extracellular space, to crosslink and form mature collagen fibrils. PICP levels (Figure 5A) were significantly higher in the AL and PL of the URA group compared with sham in all the repair groups. In the AL, PICP was highest in the URA group and was significantly different from URA+PMA (P=0.0002) and PMA (P<0.0001). Differences between URA+PMA and PMA were small and not statistically significant (P=0.7708). In the PL, PICP was highest in the URA group, with significantly higher levels compared with URA+PMA (P=0.005) and PMA (P=0.0286). There were again no differences between URA+PMA and PMA groups (P=0.8089).

PINP is challenging to measure in tissue alone, as a part of the protein is released into the blood stream as well. Thus, we measured PINP in tissue and in plasma in all groups. Tissue PINP (Figure 5B) was significantly elevated in the 3 experimental groups compared with sham. In the AL, tissue PINP was elevated in URA compared with PMA (P=0.05) but not compared with URA+PMA (P=0.9229). PINP levels in URA+PMA were significantly higher than PMA (P=0.0071). In the PL, differences between the repair groups for tissue PINP were not statistically significant. Plasma levels of PINP were not significantly different between baseline and termination, though termination levels of PINP seemed to be higher in URA and URA+PMA (Figure 5C).

Prolyl 4-Hydroxylase subunit Alpha 1 (P4HA1) levels were elevated compared with sham but were not different between the repair groups in either the anterior or posterior leaflets (Figure 5D). Heat Shock Protein 47 (HSP47) in the AL was significantly elevated in the URA group compared with URA+PMA (P=0.0005) and PMA (P=0.0078). There were no

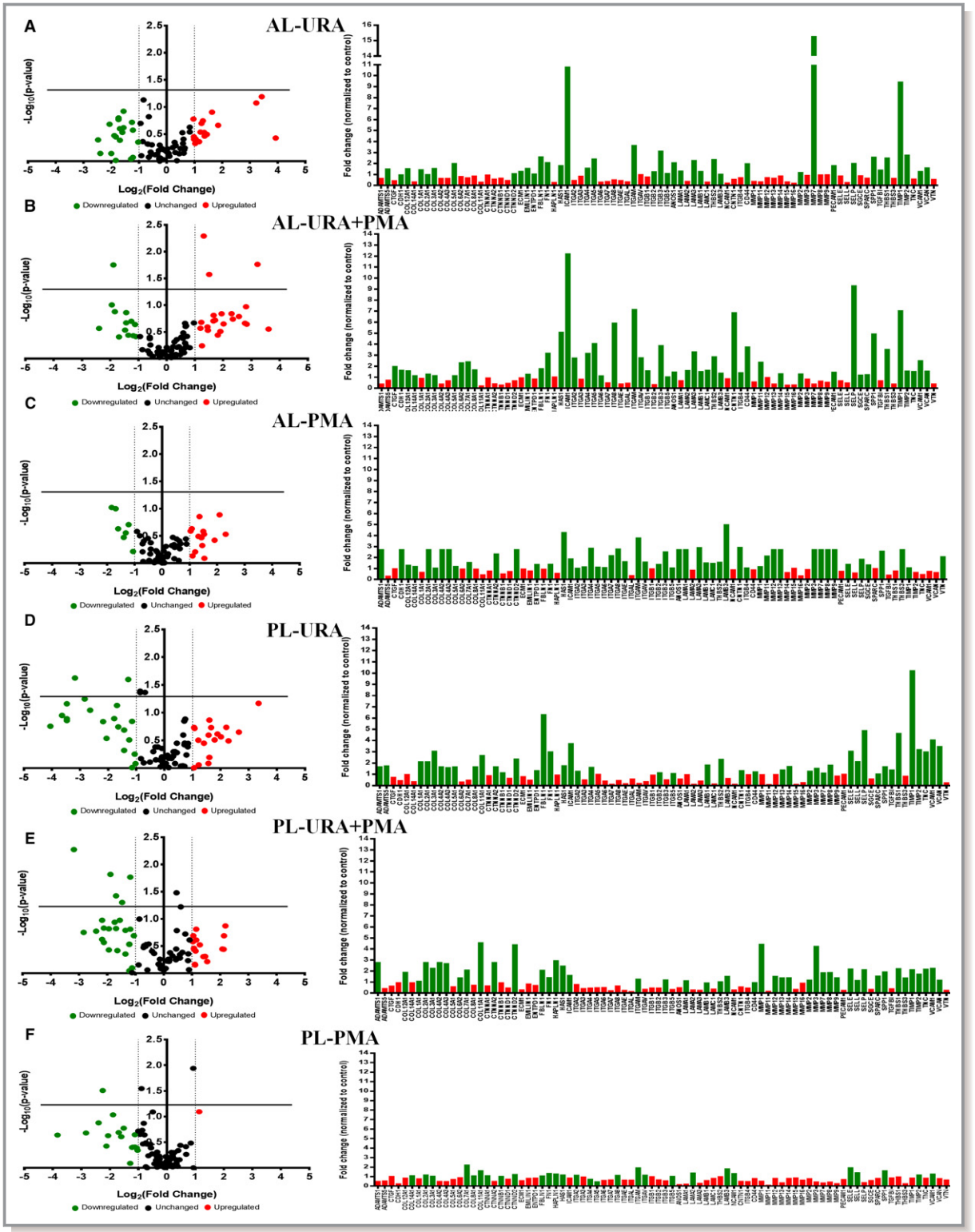

Figure 4. Gene expression studies in tissue from the anterior and posterior leaflets explanted from pigs from each experimental group, when compared with data from the sham group of animals. **A** through **C**, Differential fold change of expression of different genes in each experimental group compared with the sham group of animals in the anterior leaflet, with the significantly upregulated genes (indicated in green) and significantly downregulated genes (indicated in red) in the bar graphs. **D** through **F**, Differential expression of specific extracellular matrix and fibrosis genes between the different repairs when normalized to the sham group, with upregulated in green and downregulated in red in the bar graphs. AL indicates anterior leaflet; PL, posterior leaflet; PMA, papillary muscle approximation; URA, undersized ring annuloplasty.

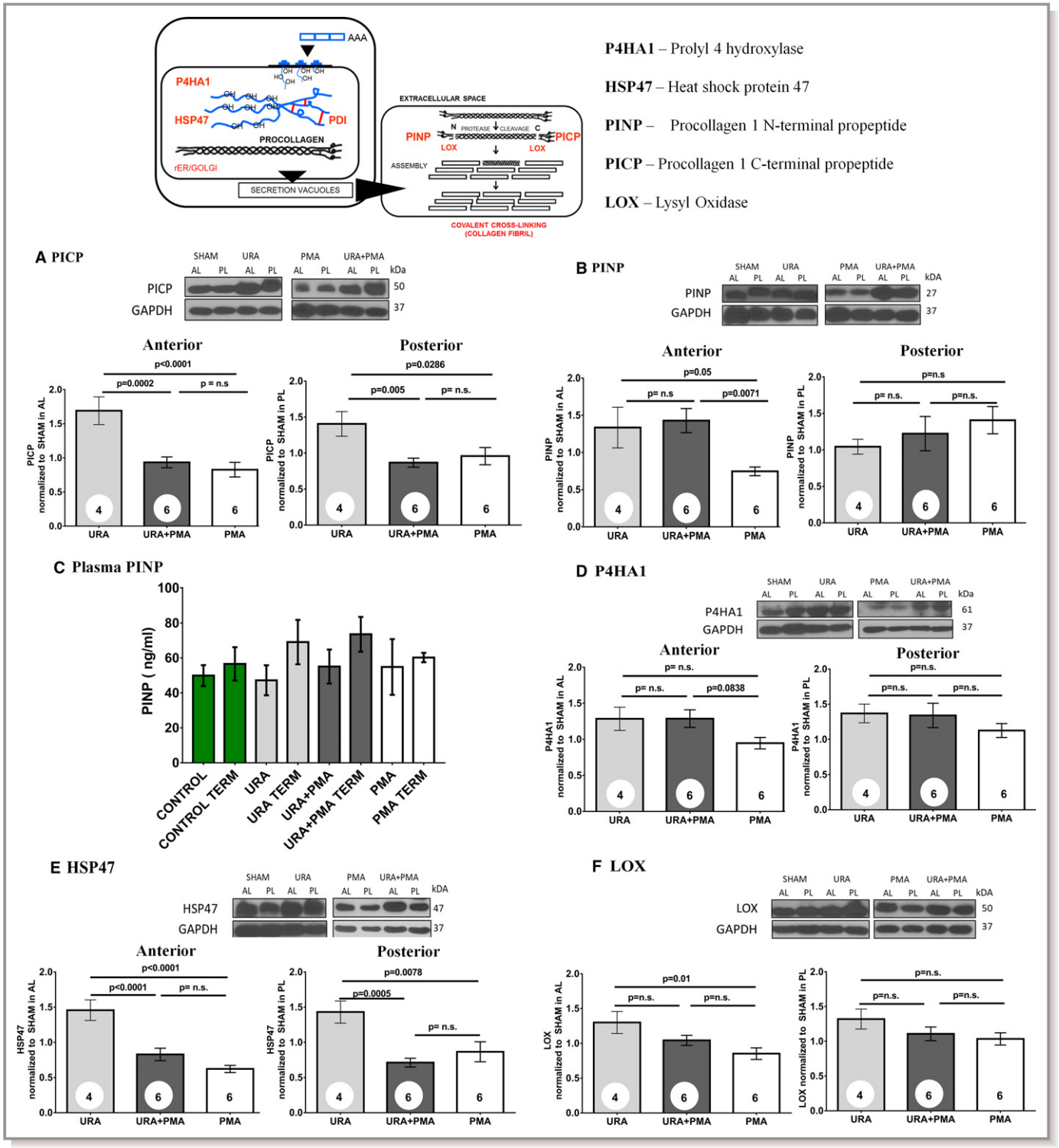

Figure 5. Protein levels in the anterior and posterior leaflets between annuloplasty (URA), combination of annuloplasty and papillary muscle approximation (URA+PMA), and papillary muscle approximation (PMA) compared with the sham group of animals. **A**, Procollagen 1 C-terminal propeptide. **B**, Procollagen 1 N-terminal propeptide. **C**, Enzyme-linked immunosorbent assay results for plasma procollagen type 1 N-terminal propeptide. **D**, Prolyl 4-hydroxylase 1. **E**, Heat shock protein 47; (**F**) Lysyl oxidase. HSP47 indicates heat shock protein 47; LO, lysyl oxidase; P4HA1, prolyl 4 hydroxylase; PICP, procollagen-1 terminal C-peptide; PINP, procollagen-1 terminal N-peptide.

differences between URA+PMA and PMA in both the leaflets (Figure 5E). Similar trends were seen in the PL as well. Lysyl oxidase (LOX) was significantly higher in URA compared with PMA (P=0.01) in the anterior leaflet but was not higher compared with URA+PMA. There were no significant differences between groups in the PL (Figure 5F).

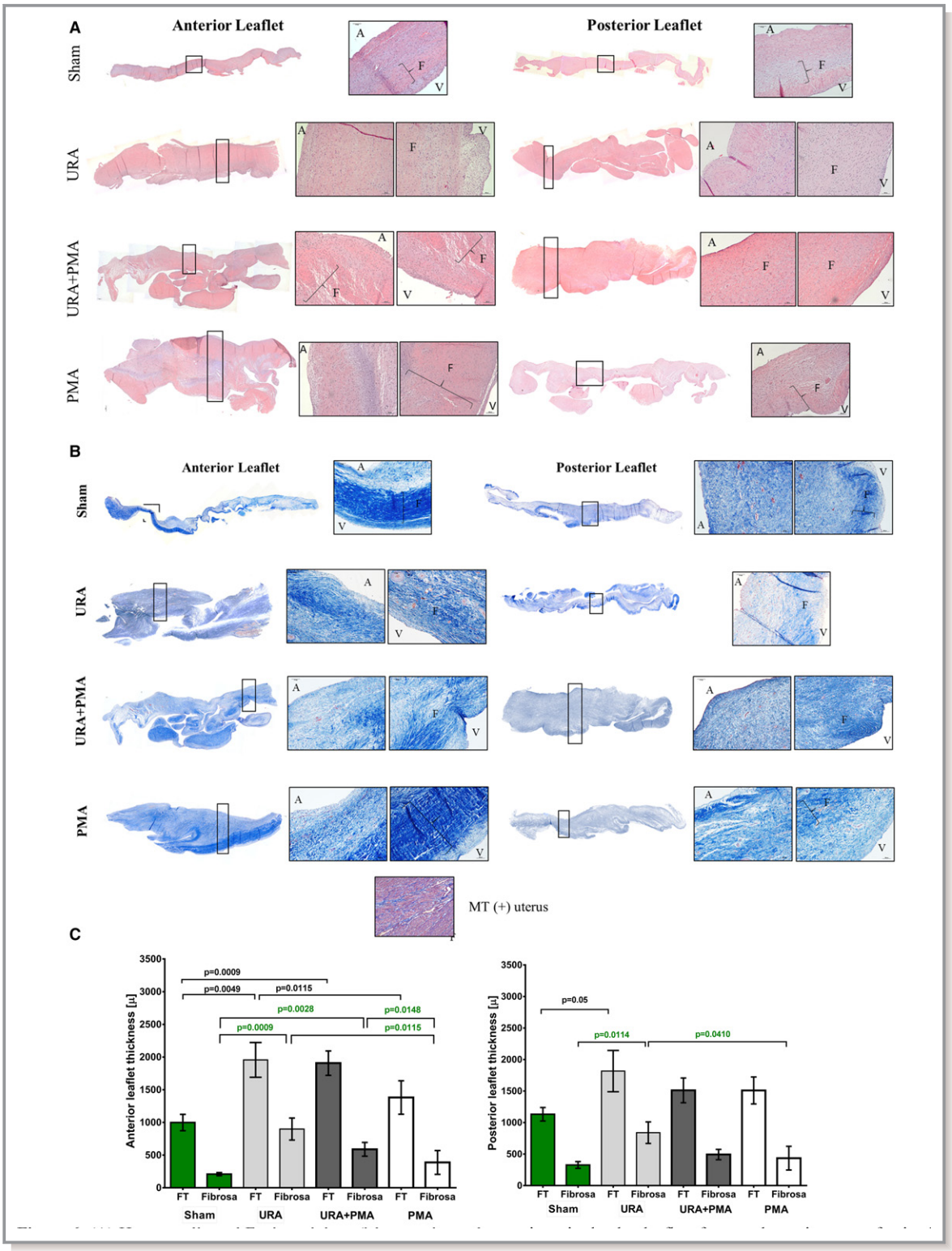

Figure 6. **A,** Hematoxylin and eosin staining of the anterior and posterior mitral valve leaflets from each repair group of animals. The anterior leaflets were thicker in all the repair groups compared with the no-repair group. The posterior leaflet was thick in the groups with annuloplasty but not in the papillary muscle approximation group. **B,** Masson's trichrome staining of the same leaflets with blue indicating collagen and red indicating muscle cells. The tri-layered structure observed in sham and papillary muscle approximation was lost in the tissues that underwent annuloplasty. **C,** Quantitative comparison of the full thickness (FT) and the fibrosa layer only between the anterior and posterior leaflets in the different groups and the sham group (shown in green). A indicates atrialis; F, fibrosa; MT, masson's trichrome; PMA, papillary muscle approximation; URA, undersized ring annuloplasty.

Histopathology of Valve Leaflets

Figure 6 depicts representative images of the AL and PL from each group, stained for hematoxylin and eosin (Figure 6A), and Masson's trichrome (MT) stain (Figure 6B). The AL and PL in the sham group of animals were thinner, with a preserved tri-layered structure (ie, atrialis, spongiosa+fibrosa, ventricularis) that is evident from both hematoxylin & eosin and Masson's trichome stains. In general, leaflets from the 3 surgical repair groups were thicker with an expanded fibrosa. In leaflets from the URA group, the distinct tri-layered structure was absent with collagen distributed through the entire leaflet cross section in the AL, and dense accumulation of collagen in the fibrosa of the PL. Similar patterns were observed in the URA+PMA group as well, with dispersion of loose collagen bundles across the entire leaflet and dense accumulation in the fibrosa layer. In the PMA group, the tri-layered structure of the leaflet seemed preserved, unlike the other 2 repair groups. Quantitative measurements of the thickness of the entire leaflet and the fibrosa alone in the anterior and posterior leaflets are shown in Figure 6C. In the anterior leaflet, the full thickness was comparable between sham and PMA, but was significantly higher in URA (P=0.0049) and URA+PMA (P=0.0009). The thickness of the anterior leaflet in the PMA group was significantly lower than in the URA group (P=0.0115). The fibrosa layer was also comparable between sham and PMA but was significantly higher in URA (P=0.0009) and URA+PMA (P=0.0028). Fibrosa in the PMA group was significantly lower than both the URA (P=0.0115) and URA+PMA groups (P=0.0148). In the posterior leaflet, the full thickness was higher in URA compared with the sham (P=0.05), and the fibrosa was thicker between sham and URA (P=0.0114). The fibrosa in the PMA group was also significantly lower than URA (P=0.0410).

Cellular Phenotype

Collagen is synthesized in cardiac valves by activated fibroblasts (myofibroblasts) that emerge from phenotypic changes in the quiescent resident fibroblasts, or from endothelial-to-mesenchymal trans-differentiation. Immunostaining was used to detect and distinguish myofibroblasts (α-SMA+) from fibroblasts (CD90+) in the AL and PL from MVs in each experimental group (Figures 7 and 8). In the sham group, expression of CD90 was significant and α-SMA was minimal in both anterior and posterior leaflets, indicative of quiescent fibroblasts. In URA and URA+PMA group, a significant and definitive overexpression of α-SMA was observed in the AL and PL, with an absence of staining for CD90. This is indicative of an activated myofibroblasts like phenotype in valvular interstitial cells. In PMA, such expression of α-SMA was not evident in either leaflet.

Transforming Growth Factor β

TGFβ is a promoter of valve cell proliferation in early stages of wound repair and is involved in phenotypic shifts in a mechanical strain dependent manner. Total and active TGFβ levels were measured in the AL and PL, depicting significant elevation in the 3 repair groups, when compared with sham (Figure 9A). Total TGFβ in the AL was not only higher in the 3 repair groups, but also significantly higher in the URA group compared with PMA (P=0.045) and URA+PMA compared with PMA (P=0.05). Such trends were not observed in the PL. The active form of TGFβ, shown in Figure 9B, was elevated among all the repair groups in the AL, and significantly different between URA+PMA and PMA (P=0.045). Such differences between repairs were not observed in the PL. Immunostaining for TGFβ, shown in Figure 9C, depicts expression only in the fibrosa layer in the sham group, but abundant and widespread expression through all the layers, except spongiosa, in the repair groups. Intensity of TGFβ staining was higher in the URA and URA+PMA groups compared with the PMA group in the anterior leaflet, but such observations were inconclusive in the PL.

Leaflet Mechanical Properties

Biaxial mechanical properties per repair group are shown in Figure 10. In the radial direction, maximum strain was highest in the PMA group (0.35±0.14, P<0.05) and equal in the URA and URA+PMA groups (0.29±0.06 and 0.29±0.01, respectively), with higher variability in the URA group. While all the groups exhibited a high degree of anisotropy, the PMA and URA+PMA groups exhibited almost half the degree of anisotropy of the URA group anterior leaflet samples (0.18±0.08, P<0.01, 0.15±0.07, and 0.34±0.01, respectively). The PMA group was also found to have the highest stiffness in the high linear region of the equibiaxial response curve in the circumferential direction, with the URA+PMA group exhibiting the lowest stiffness (62865.9±10953.4 and 7998.6±125.1 kPa, respectively). However, the URA+PMA group was found to be the stiffest in the low linear region of the equibiaxial response curve (324.8±157.3 kPa, P=0.0001) as compared with the PMA and URA groups (54.0±16.9 and 38.9±27 kPa, respectively). In the radial direction, however, the URA+PMA group was found to be the stiffest along the low linear region (14.23±5.06 kPa), with the URA group being the stiffest in the high linear region (7340.43±3287.9 kPa). Along the circumferential direction, the PL was found to be least extensible in the URA group and most extensible in the URA+PMA group (0.02, 0.04±0.014). This was also reflected in the extensibility of the radial direction as well as the maximum strain values for both the circumferential and radial directions. Unlike what was observed in the AL, the URA group was found to be the most anisotropic, compared with

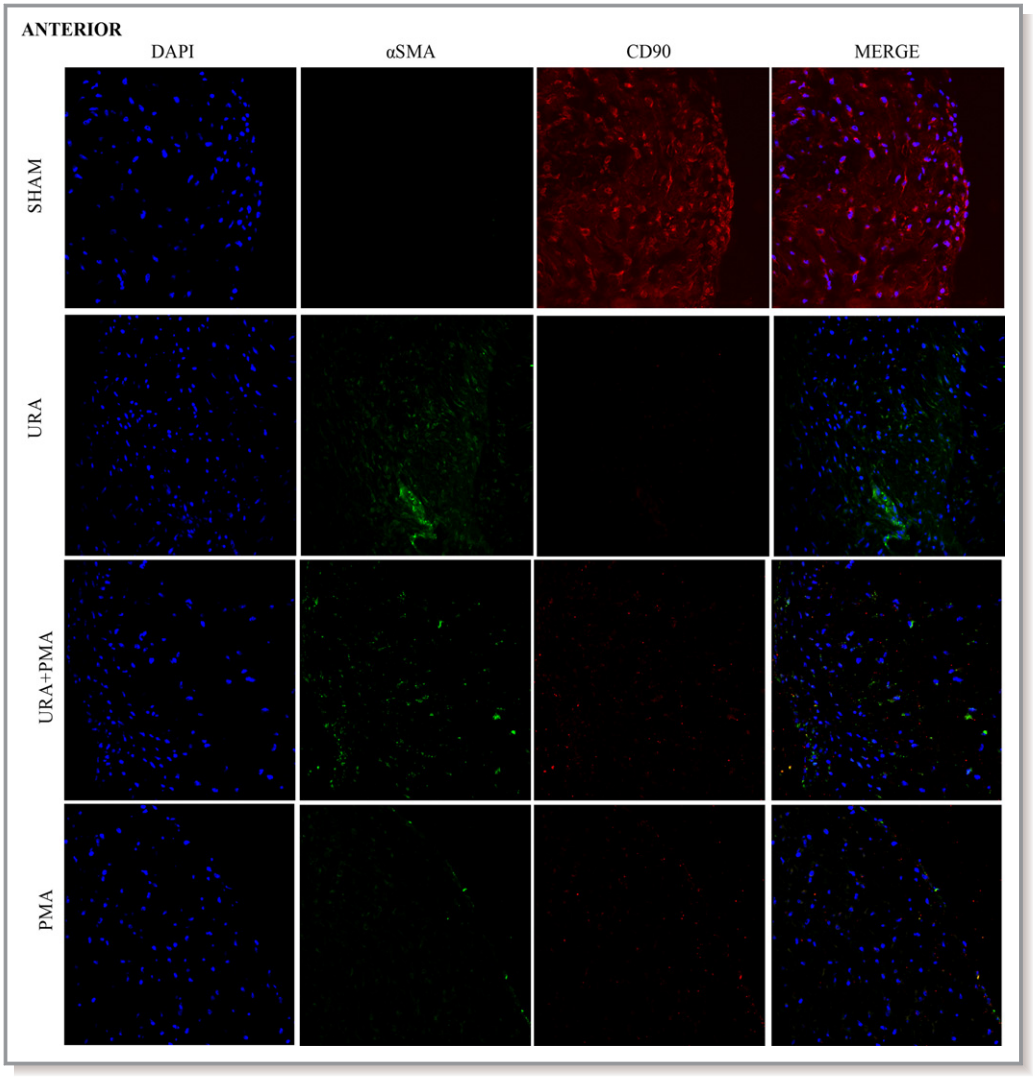

Figure 7. Immunocytochemistry images of anterior mitral valve leaflets stained for a nuclear stain-4′,6-diamidino-2-phenulindole (DAPI, blue), myofibroblast/activated fibroblast marker-α smooth muscle actin (green), quiescent fibroblast—CD90 (red). PMA indicates papillary muscle approximation; URA, undersized ring annuloplasty.

the PMA group, which was found to be the least anisotropic, although all samples exhibited high degrees of anisotropy. In both the circumferential and radial directions, the URA+PMA group was found to be the most compliant in the low linear region of the equibiaxial response curve (546.3±332.1 and 54.86±28.30 kPa, respectively). Overall, the AL was found to be more extensible than the PL, with the largest difference seen in the URA group, while leaflets in the URA+PMA and PMA groups were almost equal in extensibility in both the circumferential and longitudinal directions. The PMA and URA+PMA groups were found to have more anisotropy in the AL, while the URA group was found to have more anisotropy in the PL. The anterior and posterior leaflets of the URA group were found to have similar stiffness values along the high linear region of the circumferential direction (34106.2±22553.6 and 30414.0 kPa), although the anterior leaflet was found to be stiffer along the high linear region of the longitudinal direction (7340.4±3287.9 and 4332.2 kPa), although this trend was not preserved in the low linear region. For the URA+PMA group, the posterior leaflet was stiffer than the anterior leaflet at all points except for the high linear region of the radial direction. Conversely, the PMA group was found to have a stiffer posterior leaflet at all points except for the high linear region of the circumferential direction.

Discussion

Repair of IMR in heart failure is a complex surgery, in which the need for restoration of acute valve competence during surgery should balance the imperative for a durable repair that can sustain physiologic valve function for 10 to 30 years. Because of the motion and physical interaction of the valve

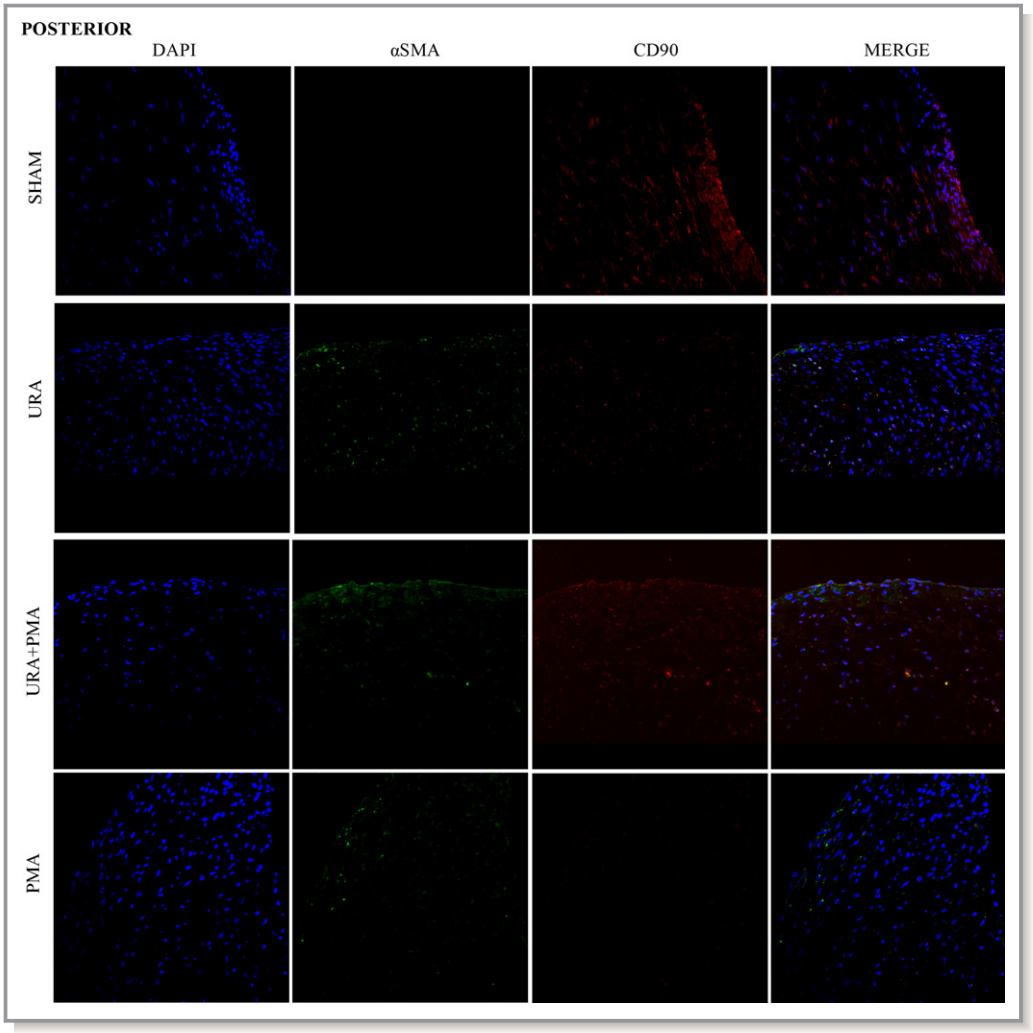

Figure 8. Immunocytochemistry images of posterior mitral valve leaflets stained for a nuclear stain-4′,6-diamidino-2-phenulindole (blue), myofibroblast/activated fibroblast marker-α smooth muscle actin (green), quiescent fibroblast—CD90 (red). PMA indicates papillary muscle approximation; URA, undersized ring annuloplasty.

leaflets in each heartbeat and the frequent changes in hemodynamic loading on the valve, the durability of the repaired valve depends upon: (1) the extent of leaflet coaptation achieved from commissure-to-commissure and the height of coaptation restored at each section of the leaflet; (2) careful reconstruction of the valve to maintain leaflet stresses and strains at near-physiologic levels and thus avoid failure along suture lines postoperatively; and (3) ensuring that the final valve geometry, function, and mechanics are restored to near-physiologic levels. These principles should minimize chronic adverse biological remodeling of the MV leaflets towards fibrosis, thickening, or calcification. The current surgical dogma has been to emphasize restoration of acute valvular competence, without much attention to restoration of physiologic valve mechanics or function in IMR. This is difficult to assess intraoperatively on the arrested heart. URA which is the most common mitral technique used for the treatment of IMR may succeed in restoring acute valve competence but may suffer from abnormal valve distortion and changes in overall force distribution resulting in an unphysiological unicuspid leaflet configuration. The PL after this repair is often vertically immobilized because of restricted posterior annular dynamics and retracted retraction into the mitral orifice and away from the 2-papillary muscle heads. The AL hyperextends towards this immobile posterior shelf and coapts onto the central belly of the PL, creating an unphysiological scenario. Because the ring draws the leaflets into the orifice, they remain tethered even in diastole. This contrasts with a normal MV scenario in which the valve leaflets have excellent mobility and do not seemed tethered in systole or diastole. In a recent study, Suh YJ demonstrated with cardiac tomography that MV leaflets in patients receiving

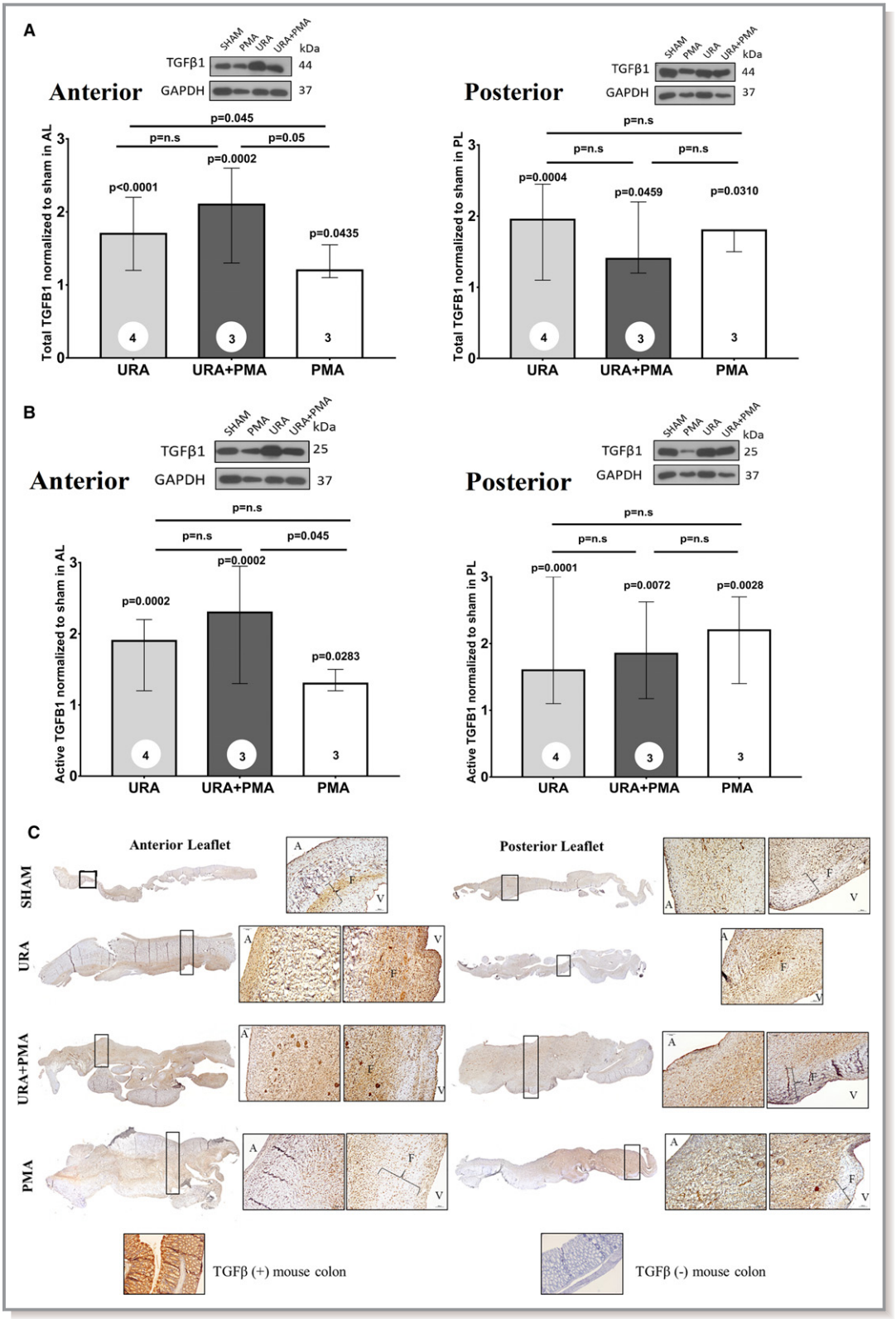

Figure 9. **A,** Comparison of total transforming growth factor-β in the mitral valve leaflets from the 3 surgical groups, when compared with the sham group and when compared with one another. **B,** Comparison of active transforming growth factor-β in the anterior and posterior mitral valve leaflets from the 3 surgical groups, when compared with the sham group and when compared with one another. **C,** Immunohistochemistry of transforming growth factor-β in leaflets from each group of animals. PMA indicates papillary muscle approximation; URA, undersized ring annuloplasty.

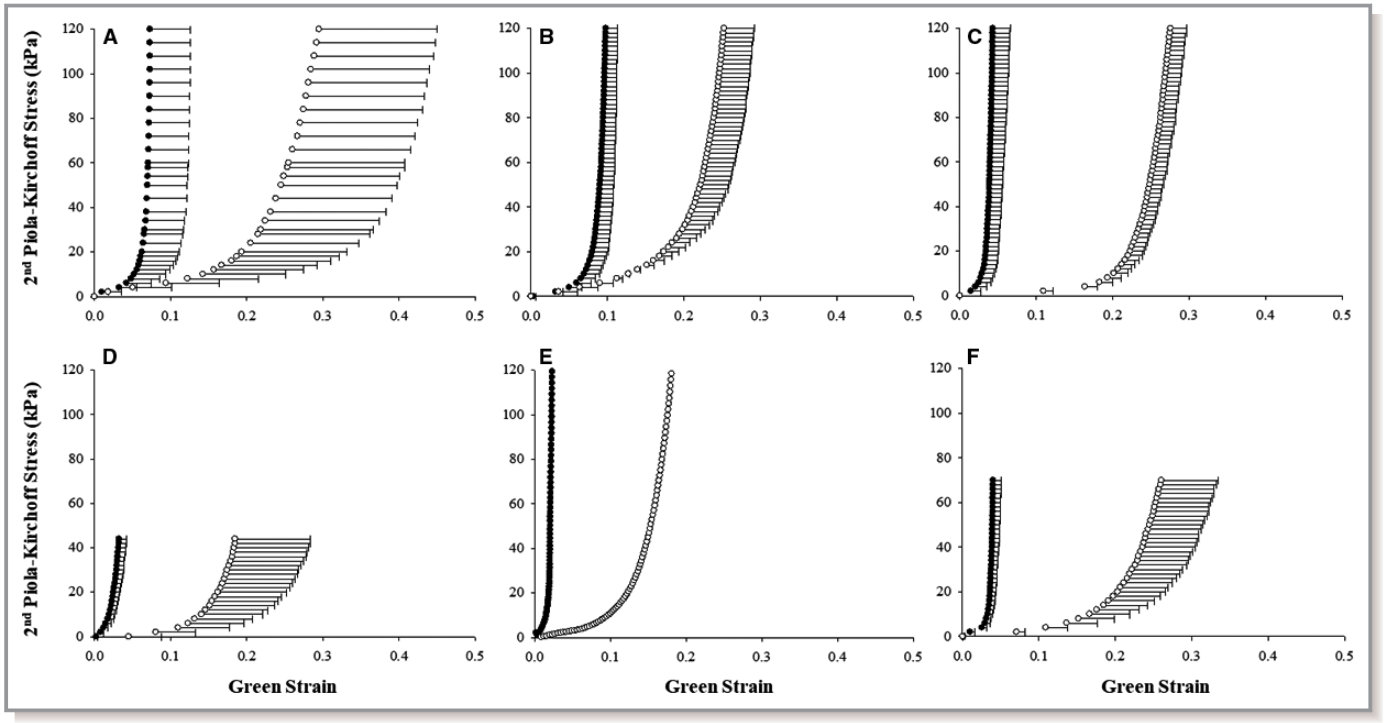

Figure 10. Biaxial stress-strain properties of the anterior and posterior mitral valve leaflets explanted from the 4 experimental groups. Equibiaxial response curves for the AML (**A** through **C**) and PML (**D** through **F**) divided into the URA (**A** and **D**), PMA (**B** and **E**) and URA+PMA (**C** and **F**) groups. The black and white curves indicate the mechanical response along the circumferential and longitudinal directions, respectively.

URA are significantly thicker within 5 years after the repair and are often associated with functional mitral stenosis and possibly some degree of calcific remodeling.[6] Cerfolio et al, in their series of MV reoperations in 49 consecutive patients after initial URA, reported that 22 of the patients presented with leaflet fibrosis and calcification, while most of the remaining patients had ring or suture dehiscence.[5]

The present experimental study, to our knowledge for the first time, convincingly demonstrates that the unphysiological leaflet kinematics after mitral repair for IMR with URA elevates collagen synthesis in both the AL and PL, markedly elevates markers of activated myofibroblasts, with a parallel increase in transforming growth factor β in the leaflets. These biological changes seem to parallel changes in the mechanical properties of the leaflets within a short span of 3 months after repair. When the leaflet kinematics were improved slightly by addition of PMA to the URA, inhibition or changes in the biological consequences were limited, but if the leaflet kinematics were markedly restored with a PMA the pathogenic biological changes could be largely inhibited. Levels of collagen and the chaperones involved in synthesis of new collagen molecules and their extracellular cross linkage and maturation, were significantly lower in leaflets from PMA compared with URA or URA+PMA. The distinct differences in cellular activation and TGFβ levels in the leaflets are evident, hinting at the involvement of a stretch sensitive pathway. Merryman et al demonstrated synergy between cyclic tension and TGFβ in aortic valve interstitial cells using an ex vivo cell culture experiment, with higher levels of strain resulting in elevated amounts of TGFβ within 7 to 14 days.[23] Their study also demonstrated that interstitial cells in this abnormal mechanical environment were positive for biosynthetic proteins. Walker et al studied the interaction between TGFβ and valve interstitial cells, and demonstrated that the quiescent fibroblast like cells in the valves are activated in the presence of TGFβ and change in their phenotype to myofibroblast like cells that promote alterations in the valve matrix architecture.[24] Yip and colleagues demonstrated that activated cells that remodel their immediate microenvironments by depositing more collagen, respond to the increased matrix stiffness with local calcification.[25] Though all these preceding studies were performed using aortic valve cells, it is reasonable to expect similar signaling and pathways in MV cells as well. Evidence of MV leaflets to adversely remodel and lead to fibrosis was reported by Dal-Bianco et al in a series of preclinical reports.[12] Unlike the post-repair leaflet remodeling focus of this work, their work emphasized the earliest changes in the tethered MV leaflets after an myocardial infarction. Their study demonstrated that mechanical stretch from valve tethering after an infarction could elicit early changes in valve biology, which is worsened when exposed to

inflammatory cytokines from the ischemic myocardium. TGFβ was elevated in these valves as well, which could be modulated by treating the valves with losartan (a downstream TGFβ inhibitor). This prior art, taken along with our novel findings, open avenues to use drugs to modify and maintain valve biology after a surgical repair, which could better explain mechanobiology of heart valves and have significant clinical impact.

Study Limitations

The novel findings of this work should be considered with some limitations of the methods that are part of any experimental design. A single annuloplasty ring shape was considered in this experiment, while clinically a multitude of shapes and sizes are used. Furthermore, this study only demonstrated that the leaflets were tethered after annuloplasty but did not compute leaflet stresses and warrants further investigation in this direction. This study was limited to a 3-month postsurgical follow-up, which was chosen arbitrarily to investigate the biological changes, and may be too short to link biological changes to clinical outcomes. The significant biological changes measured at this timepoint, indicate that earlier measurements can provide insights into the inciting signaling cascades, while a more chronic study investigating tissues at a later stage might demonstrate significant thickening and calcification of the valves and impair valve function. This study was also limited to specific cellular markers, whereas an unbiased flow cytometry study to evaluate cell populations would provide insights into the network of cells and their signaling that is involved in the pathogenic processes. In this study, gene expression studies were also confined to extracellular matrix proteins only and normalized to sham and use of unbiased RNA-seq can provide deeper insights. Nonetheless, these limitations do not in any manner reduce the impact of the proposed work, which convincingly demonstrates a link between post-repair leaflet mechanics and the chronic biological changes in the valve.

Conclusions

Abnormal biomechanics imposed on the MV by a surgical repair are associated with pathogenic biological changes in the MV leaflets within a short period of 3 months in this swine experimental model of moderate IMR. Collagen levels were elevated in these stressed leaflets, which could be avoided if a repair preserved/restored physiologic leaflet mechanics. The profibrotic changes in the valve paralleled increase in TGF-β and cellular phenotypic shifts, which provide a potential signaling pathway to target with drugs.

Sources of Funding

This work was partially supported by grant awards to Dr Padala from the American Heart Association (14SDG20380081), the National Heart Lung and Blood Institute (1R01HL135145-01A1, 1R01HL133667-01A1, 1R01HL140325-01A1), and the Carlyle Fraser Heart Center at Emory University Hospital Midtown. Dr Sielicka was supported by a post-doctoral fellowship grant from the American Heart Association (17POST33680072).

Disclosures

Dr Thourani reports consulting or other relationships with Abbott Vascular, Edwards Lifesciences, W. L. Gore, Boston Scientific, and JenaValve. Dr Sarin reports relationships with Medtronic, and W.L. Gore. The remaining authors have no disclosures to report.

References

1. Bach DS, Bolling SF. Improvement following correction of secondary mitral regurgitation in end-stage cardiomyopathy with mitral annuloplasty. *Am J Cardiol*. 1996;78:966–969.
2. Bertrand PB, Verbrugge FH, Verhaert D, Smeets CJ, Grieten L, Mullens W, Gutermann H, Dion RA, Levine RA, Vandervoort PM. Mitral valve area during exercise after restrictive mitral valve annuloplasty: importance of diastolic anterior leaflet tethering. *J Am Coll Cardiol*. 2015;65:452–461.
3. Gelsomino S, van Garsse L, Luca F, Lorusso R, Cheriex E, Rao CM, Caciolli S, Vizzardi E, Crudeli E, Stefano P, Gensini GF, Maessen J. Impact of preoperative anterior leaflet tethering on the recurrence of ischemic mitral regurgitation and the lack of left ventricular reverse remodeling after restrictive annuloplasty. *J Am Soc Echocardiogr*. 2011;24:1365–1375.
4. Zhu F, Otsuji Y, Yotsumoto G, Yuasa T, Ueno T, Yu B, Koriyama C, Hamasaki S, Biro S, Kisanuki A, Minagoe S, Levine RA, Sakata R, Tei C. Mechanism of persistent ischemic mitral regurgitation after annuloplasty: importance of augmented posterior mitral leaflet tethering. *Circulation*. 2005;112:I396–I401.
5. Cerfolio RJ, Orzulak TA, Pluth JR, Harmsen WS, Schaff HV. Reoperation after valve repair for mitral regurgitation: early and intermediate results. *J Thorac Cardiovasc Surg*. 1996;111:1177–1183; discussion 1183–1174.
6. Suh YJ, Chang BC, Im DJ, Kim YJ, Hong YJ, Hong GR, Kim YJ. Assessment of mitral annuloplasty ring by cardiac computed tomography: correlation with echocardiographic parameters and comparison between two different ring types. *J Thorac Cardiovasc Surg*. 2015;150:1082–1090.
7. Kunzelman KS, Quick DW, Cochran RP. Altered collagen concentration in mitral valve leaflets: biochemical and finite element analysis. *Ann Thorac Surg*. 1998;66:S198–S205.
8. Quick DW, Kunzelman KS, Kneebone JM, Cochran RP. Collagen synthesis is upregulated in mitral valves subjected to altered stress. *ASAIO J*. 1997;43:181–186.
9. Grande-Allen KJ, Barber JE, Klatka KM, Houghtaling PL, Vesely I, Moravec CS, McCarthy PM. Mitral valve stiffening in end-stage heart failure: evidence of an organic contribution to functional mitral regurgitation. *J Thorac Cardiovasc Surg*. 2005;130:783–790.
10. Grande-Allen KJ, Borowski AG, Troughton RW, Houghtaling PL, Dipaola NR, Moravec CS, Vesely I, Griffin BP. Apparently normal mitral valves in patients with heart failure demonstrate biochemical and structural derangements: an extracellular matrix and echocardiographic study. *J Am Coll Cardiol*. 2005;45:54–61.
11. Dal-Bianco JP, Aikawa E, Bischoff J, Guerrero JL, Handschumacher MD, Sullivan S, Johnson B, Titus JS, Iwamoto Y, Wylie-Sears J, Levine RA, Carpentier A. Active adaptation of the tethered mitral valve: insights into a compensatory mechanism for functional mitral regurgitation. *Circulation*. 2009;120:334–342.
12. Dal-Bianco JP, Aikawa E, Bischoff J, Guerrero JL, Hjortnaes J, Beaudoin J, Szymanski C, Bartko PE, Seybolt MM, Handschumacher MD, Sullivan S, Garcia

ML, Mauskapf A, Titus JS, Wylie-Sears J, Irvin WS, Chaput M, Messas E, Hagege AA, Carpentier A, Levine RA; Leducq Transatlantic Mitral Network. Myocardial infarction alters adaptation of the tethered mitral valve. *J Am Coll Cardiol*. 2016;67:275–287.

13. Shapero K, Wylie-Sears J, Levine RA, Mayer JE Jr, Bischoff J. Reciprocal interactions between mitral valve endothelial and interstitial cells reduce endothelial-to-mesenchymal transition and myofibroblastic activation. *J Mol Cell Cardiol*. 2015;80:175–185.
14. Bartko PE, Dal-Bianco JP, Guerrero JL, Beaudoin J, Szymanski C, Kim DH, Seybolt MM, Handschumacher MD, Sullivan S, Garcia ML, Titus JS, Wylie-Sears J, Irvin WS, Messas E, Hagege AA, Carpentier A, Aikawa E, Bischoff J, Levine RA; Leducq Transatlantic Mitral Network. Effect of losartan on mitral valve changes after myocardial infarction. *J Am Coll Cardiol*. 2017;70:1232–1244.
15. Padala M, Gyoneva LI, Thourani VH, Yoganathan AP. Impact of mitral valve geometry on hemodynamic efficacy of surgical repair in secondary mitral regurgitation. *J Heart Valve Dis*. 2014;23:79–87.
16. Shi W, McIver BV, Kalra K, Sarin EL, Schmarkey S, Duggan M, Thourani VH, Guyton RA, Padala M. A swine model of percutaneous intracoronary ethanol induced acute myocardial infarction and ischemic mitral regurgitation. *J Cardiovasc Transl Res*. 2017;10:391–400.
17. Padala M. Papillary muscle approximation is an anatomically correct repair for ischemic mitral regurgitation. *J Am Coll Cardiol*. 2016;68:1146–1147.
18. Padala M, Kalra K, Shi W, Wang Q, Guyton RA, Sun W, Thourani VH, Sarin EL. Intra-ventricular papillary muscle banding vs. Undersized mitral annuloplasty to treat ischemic mitral regurgitation in a chronic swine model. *Circulation*. 2014;130:A18607.
19. Rama A, Praschker L, Barreda E, Gandjbakhch I. Papillary muscle approximation for functional ischemic mitral regurgitation. *Ann Thorac Surg*. 2007;84:2130–2131.
20. Shingu Y, Yamada S, Ooka T, Tachibana T, Kubota S, Tsutsui H, Matsui Y. Papillary muscle suspension concomitant with approximation for functional mitral regurgitation. *Circ J*. 2009;73:2061–2067.
21. Sarin EL, Shi W, Duara R, Melone TA, Kalra K, Strong A, Girish A, McIver BV, Thourani VH, Guyton RA, Padala M. Swine (Sus scrofa) as a model of postinfarction mitral regurgitation and techniques to accommodate its effects during surgical repair. *Comp Med*. 2016;66:290–299.
22. Sacks MS, Sun W. Multiaxial mechanical behavior of biological materials. *Annu Rev Biomed Eng*. 2003;5:251–284.
23. Merryman WD, Lukoff HD, Long RA, Engelmayr GC Jr, Hopkins RA, Sacks MS. Synergistic effects of cyclic tension and transforming growth factor-beta1 on the aortic valve myofibroblast. *Cardiovasc Pathol*. 2007;16:268–276.
24. Walker GA, Masters KS, Shah DN, Anseth KS, Leinwand LA. Valvular myofibroblast activation by transforming growth factor-beta: implications for pathological extracellular matrix remodeling in heart valve disease. *Circ Res*. 2004;95:253–260.
25. Yip CY, Chen JH, Zhao R, Simmons CA. Calcification by valve interstitial cells is regulated by the stiffness of the extracellular matrix. *Arterioscler Thromb Vasc Biol*. 2009;29:936–942.